

Timing analysis of the isolated neutron star RX J0720.4-3125[★]

Silvia Zane¹, Frank Haberl², Mark Cropper¹, Vyacheslav E. Zavlin², David Lumb³, Steve Sembay⁴ and Christian Motch⁵

¹ Mullard Space Science Lab, University College London, Holmbury St. Mary, Dorking, Surrey, RH5 6NT, UK

² Max Planck Institut für Extraterrestrische Physik, Giessenbachstrasse, D-85748 Garching, Germany

³ Space Science Department, ESTEC, Postbus 299, Keplerlaan 1, Noordwijk 2200 AG, The Netherlands

⁴ X-ray Astronomy Group, Department of Physics and Astronomy, University of Leicester, Leicester LE1 7RH, UK

⁵ Observatoire Astronomique, CNRS UMR 7550, 11 Rue de l'Université, F-67000 Strasbourg, France

Received:

ABSTRACT

We present a combined analysis of *XMM-Newton*, *Chandra* and *Rosat* observations of the isolated neutron star RXJ0720.4-3125, spanning a total period of ~ 7 years. We develop a maximum likelihood periodogramme for our analysis based on the ΔC -statistic and the maximum likelihood method, which are appropriate for the treatment of sparse event lists. Our results have been checked *a posteriori* by folding a further *BeppoSAX*-dataset with the period predicted at the time of that observation: the phase is found to be consistent.

The study of the spin history and the measure of the spin-down rate is of extreme importance in discriminating between the possible mechanisms suggested for the nature of the X-ray emission. The value of \dot{P} , here measured for the first time, is $\approx 10^{-14}$ s/s. This value can not be explained in terms of torque from a fossil disk. When interpreted in terms of dipolar losses, it gives a magnetic field of $B \approx 10^{13}$ G, making also implausible that the source is accreting from the underdense surroundings. On the other hand, we also find unlikely that the field decayed from a much larger value ($B \approx 10^{15}$ G, as expected for a magnetar powered by dissipation of a superstrong field) since this scenario predicts a source age of $\approx 10^4$ yrs, too young to match the observed X-ray luminosity. The observed properties are more compatible with a scenario in which the source is $\approx 10^6$ yrs old, and its magnetic field has not changed substantially over the lifetime.

Key words: Stars: neutron; stars: oscillations; pulsars: general; magnetic fields.

1 INTRODUCTION

RXJ0720.4-3125 is a nearby, isolated neutron star (NS) that was originally discovered with ROSAT during a systematic survey of the galactic plane (Haberl et al., 1997). The source exhibits all the common characteristics of the other six ROSAT NS candidates (hereafter dim NSs, see e.g. Treves et al., 2000 for a review): a blackbody-like, soft spectrum with $kT \sim 80$ eV; an exceedingly large X-ray to optical flux ratio; a low X-ray luminosity, $L_X \approx 10^{30} - 10^{31}$ erg s⁻¹; a low column density and no evidence for a binary compan-

ion. An optical counterpart has been identified (Motch & Haberl, 1998; Kulkarni & van Kerkwijk, 1998).

Pulsation associated with the spin period has been observed in four dim NSs: RXJ0720.4-3125 ($P \approx 8.39$ s), RXJ0420.0-5022 ($P \approx 22.69$ s), RXJ0806.4-4123 ($P \approx 11.37$ s) and RBS1223 ($P \approx 5.16$ s). The pulse shape of RXJ0720.4-3125 is almost sinusoidal (Haberl et al., 1997; Cropper et al., 2001).

The true nature of the mechanism powering the X-ray emission from dim NSs is still unclear. Until a few years ago, these sources were thought to constitute a stand alone class and two mechanisms were proposed for their emission: either accretion from the interstellar medium onto an old neutron star or release of thermal radiation from a younger, cooling object (see e.g. Pavlov et al., 1996; Treves et al.,

[★] Based on observations obtained with *XMM-Newton*, an ESA science mission with instruments and contributions directly funded by ESA Member States and the USA (NASA).

2000; Motch, 2001 and references therein). More recently, it has been noted that the period of RXJ0720.4-3125 is somewhat unusual and falls in the very narrow range in which the anomalous X-ray pulsars (AXPs) periods cluster ($P \sim 6-12$ s, see e.g. Mereghetti, 2000). This hints at a possible evolutionary link between dim NSs, AXPs, and soft gamma-ray repeaters (SGRs, see e.g. Heyl & Kulkarni, 1998; Heyl & Hernquist, 1998; Colpi et al., 2000; Alpar, 1999, 2000, 2001). Two kind of “unified” scenarios have been then proposed. In the first one, the common mechanism powering the three classes of objects is dissipation of a decaying, superstrong magnetic field ($B \gtrsim 10^{14} - 10^{15}$ G). In this case dim NSs represent the descendants of SGRs and AXPs, and RXJ0720.4-3125 may be one of the closest old magnetars. Alternatively, all three classes may contain neutron stars with lower (canonical) magnetic field ($B \approx 10^{12}$ G) endowed by a fossil disk (Alpar, Ankay & Yazgan, 2001; Alpar, 2001). In this interpretation, dim NSs would be in the propellor phase and would be the progenitors of AXPs and SGRs, the latter having entered an accretion phase.

In any model involving magnetars, proton cyclotron features are expected to lie in the X-ray range, while electron cyclotron lines are expected in the same band for canonical magnetic field. According to Zane et al. (2001), for surface magnetic fields strengths of $\sim 10^{14} - 10^{15}$ G spectra exhibit a distinctive absorption feature at the proton cyclotron energy $\sim 0.63(B/10^{14} \text{ G})$ keV. The required resolving power is ≈ 100 , therefore the detection of this feature is well within the capabilities of *XMM-Newton* grating spectrometers. Recently, Paerels et al. (2001) have presented spectra of RXJ0720.4-3125 using *XMM-Newton*, and found that there is no evidence for absorption lines and edges in the X-ray spectrum. Unless different atmospheric effects may concur in suppressing the feature, when taken straightforward the absence of electron or proton cyclotron resonances in the RGS band excludes a range of average magnetic field strengths, $B \approx (0.3 - 2) \times 10^{11}$ G and $(0.5 - 2) \times 10^{14}$ G.

Based on the same *XMM-Newton* observation, Cropper et al. (2001) presented the pulse-shape analysis of RXJ0720.4-3125, modelling spin pulse intensity and hardness ratio profiles. By assuming that the source of the flux variation is the changing visibility of the heated magnetic polar caps, they derived an upper limit on the cap size and showed that a polar cap larger than $\sim 60^\circ - 65^\circ$ can be rejected at a confidence level of 90%. Whatever the mechanism, the X-ray emitting region is therefore confined to a relatively small fraction of the star surface. It is worth noticing that such a small hot region can not be explained only in terms of non-uniformity in the distribution of the surface cooling temperature induced by an high magnetic field (Greenstein & Hartke 1983; Page 1995). The temperature gradient which is induced by the B -dependence of the thermal conductivity of the neutron star crust is relatively smooth and, even in the (unrealistic) limit case $B \rightarrow \infty$ the associated blackbody luminosity drops only by a factor 1/2 at $\sim 60^\circ$ and by an order of magnitude at $\sim 77^\circ$. By performing pulse phase spectroscopy, Cropper et al. (2001) also found that the observed hardness ratio is softest slightly before flux maximum. The same characteristic was later discovered by Perna et al. (2001) in the spectra of AXPs. Cropper et al. (2001) suggested two possible explanations for this effect: their best-fitting model is based on radiation beam-

ing, while an alternative one assumes a spatially variable absorbing matter, co-rotating in the magnetosphere. The latter may be indeed the case if the star is propelling matter outward (Alpar, Ankay & Yazgan 2001).

Further information about the nature of this puzzling source can be obtained by the spin history. In magnetars magneto-dipolar radiation will cause rapid spin-down at a rate $\dot{P} \approx 10^{-11} (B/10^{14} \text{ G})^2 / P \text{ ss}^{-1}$, and it has been the positive detection of a secular spin-down of this order that has suggested the association of AXPs and SGRs with ultra-magnetized NSs (Kouveliotou et al., 1998, 1999; Thompson et al., 2001). The preliminary measure of \dot{P} published by Haberl et al. (1997) for RXJ0720.4-3125 is uncertain to a considerably large value, and does not allow spin-up and spin-down to be discriminated. Very recently, Hambaryan et al. (2002) presented the *first evidence of large spin-down rate* in a dim NS, RBS1223. Their measure is partially based on ROSAT data where the detection of the period was not highly significant, and also the value ($\dot{P} = 1.35_{-0.67}^{+0.69} \times 10^{-11}$ s/s) is still compatible with being due to torque from a fossil disk. However, it is certainly worth noticing that, when taken face value and interpreted in terms of dipolar rotational losses, this implies the presence of a superstrong magnetic field, $B \approx (3.5 - 6.5) \times 10^{14}$ G.

A similar measure of \dot{P} for the closest pulsating candidate, RXJ0720.4-3125, is therefore of extreme importance, as well as the accurate tracking of its spin history.

This is the first opportunity to investigate the pulse timing in the *XMM-Newton* data, since at the time of the previous papers (Paerels et al. 2001, Cropper et al., 2001) the timing correlation files were not sufficiently well determined. Here we present a combined analysis of *XMM-Newton*, *Chandra* and *Rosat* data, spanning a period of ~ 7 years.

2 OBSERVATIONS

The log of observations used for this study is given in Table 1.

RXJ0720.4-3125 has been observed twice by *XMM-Newton*: first on 2000 May 13, during the Calibration/Performance Verification phase (Paerels et al. 2001, Cropper et al. 2001) and later on 21 November 2001, again for calibrations. For the analysis presented in this paper we have used data from all three EPIC cameras on both epochs. The data were reduced using the *XMM-Newton* Scientific Analysis System (SAS) version 5.1. Source counts in the range 0.12 to 1.2 keV (PN) and 0.1 to 2.0 keV (MOS) were extracted in an aperture of 40 arcsec for the PN X00a, 30 arcsec for PN X00b, and 30 arcsec for the MOS cameras. Events with patterns 0-4 (single and double events) were selected for MOS, while patterns 0-12 (all the valid PN patterns) were retained for PN. Data arriving during episodes of high background which were experienced in the 2000 May 13 observation were excluded. Also in this observation, some PN event times were noted not to be integer multiple of the frame times, but delayed by 1 second: such events (in total about 34 ks from the 50 ks) were corrected in the event list. Finally, times were converted to Barycentric Dynamical Time (TDB) at solar system barycentre.

The *Chandra* observations were made over three days

Date	Observatory	Instrument	Exposure identification	Exposure duration (s)	Effective exposure (s)	Label
1993 Sep 27	<i>Rosat</i>	PSPC	rp300338n00	11980	3221	R93
1996 Apr 25	<i>Rosat</i>	HRI	rh300508n00	7838	3566	R96a
1996 May 7	<i>Rosat</i>	HRI	rh180100n00	7743	3125	R96b
1996 Sep 27	<i>Rosat</i>	HRI	rh300508a01	1498	1409	R96c
1996 Nov 3	<i>Rosat</i>	HRI	rh400884n00	65698	33569	R96d
1998 Sep 27	<i>Rosat</i>	HRI	rh400944n00	460195	3566	R98
2000 Feb 1	<i>Chandra</i>	HRC-S(LETG 1st order)	348+349+745	305528	37635	Ch00
2000 May 13	<i>XMM-Newton</i>	MOS1 + thin filter	0124100101-001	61648	61648	X00a
		MOS2 + thin filter	0124100101-002	61648	61648	
		PN + thin filter	0124100101-003	62425	62425	
2000 Nov 21	<i>XMM-Newton</i>	MOS1 + medium filter	0132520301-007	17997	17997	X00b
		MOS2 + medium filter	0132520301-008	17994	17994	
		PN + medium filter	0132520301-003	25651	25651	
1997 Mar 16	<i>BeppoSAX</i>	LECS	LECS_20079001	99418		S97

Table 1. The ROSAT, Chandra and XMM-Newton observations of RXJ0720.4-3125 used in this paper.

starting on 2000 Feb 1 using the HRC-S with LETG. The events were extracted from zero-order images of the source (namely, from circles of 2 arcsec radius centered at the star’s position). The dispersed data (1st and higher orders) are strongly contaminated by background (about 50-60%) and are not useful for this task. On the other hand, the background contamination in the zero-order data is negligible, about 2-3%. Also, the zero-order data are not piled-up: this effect can appear only at larger count rates ($\sim 10^5$ ct/s).

The *Rosat* observations were taken over a period of five years in 1993, 1996 and 1998. An earlier report of the analysis of the 1993 and 1996 data is in Haberl et al. (1997). The data were re-extracted and re-analysed using the EXSAS software system to make use of the most recent knowledge of spacecraft clock corrections. The 1998 data were taken shortly before a spacecraft emergency safe-hold, and do not benefit from a clock calibration: timing corrections are therefore extrapolated from the last available calibration. Timings may therefore be incorrect up to several seconds (W. Becker, private communication): this means that the reference of this observation to the rest of the dataset is problematic. However, no significant drifts are expected over the duration of the observation itself, so that the data are still useful in a standalone analysis.

Although the countrate is too low for our main analysis, we have also extracted the SAX LECS observation of RX J0720.4–3125 from the SAX data archive (the source was not visible in the other SAX instruments) for use as an *a posteriori* check on our derived timing parameters. Here we used the event list from the pipeline, correcting the times to the solar system barycentre using the FTOOL earth2sun. This neglects the light travel time from Earth centre to the satellite in low Earth orbit, ~ 20 ms, which is negligible for the purposes of our *a posteriori* check.

The major datasets in Table 1 are from the two XMM-Newton observations which have high count-rates (particularly the EPIC-PN), and the long 1996 Nov 3 *Rosat* data. The 1998 *Rosat* and the *Chandra* observations are valuable by nature of their several day durations.

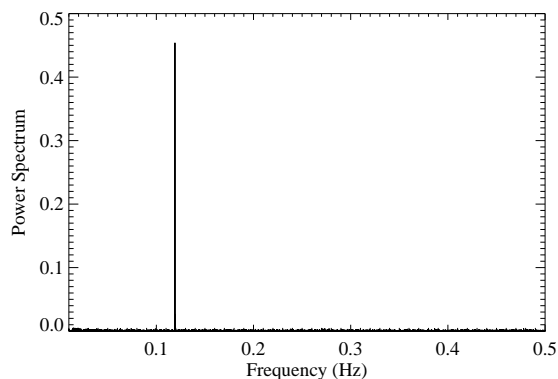


Figure 1. The Rayleigh transform of the X00a PN dataset over the period range 100 s to 2 s. This shows only the single frequency at 8.391 s (0.11917 Hz), as reported in Haberl et al. (1997).

3 TIME SERIES ANALYSIS

Our data originate from instrumentation with widely differing sensitivities: typical count rates vary from 1 count every ~ 3 s for *Rosat* HRI to ~ 6 counts/s for XMM-Newton PN. However, none of these count rates is sufficiently high for a normal distribution of counts to be expected in a time bin of adequate time resolution. The body of literature addressing discrete Fourier Transforms (for example Deeming 1975, Scargle 1982, Schwarzenberg-Czerny 1998) is not directly applicable for our analysis. The treatment of sparse data and event list data is generally accomplished using the Rayleigh Transform (for example de Jager 1991, Mardia 1972). It should be noted that this transform is numerically the same as the discrete Fourier Transform.

It will be important in our analysis to define confidence intervals to the derived quantities, in particular the period. In the case where sufficient counts per sample are available, this is generally achieved by least squares fits to the data (for example Kurtz 1985), but this is not possible for sparse or event list data. In this case it is necessary to use the more

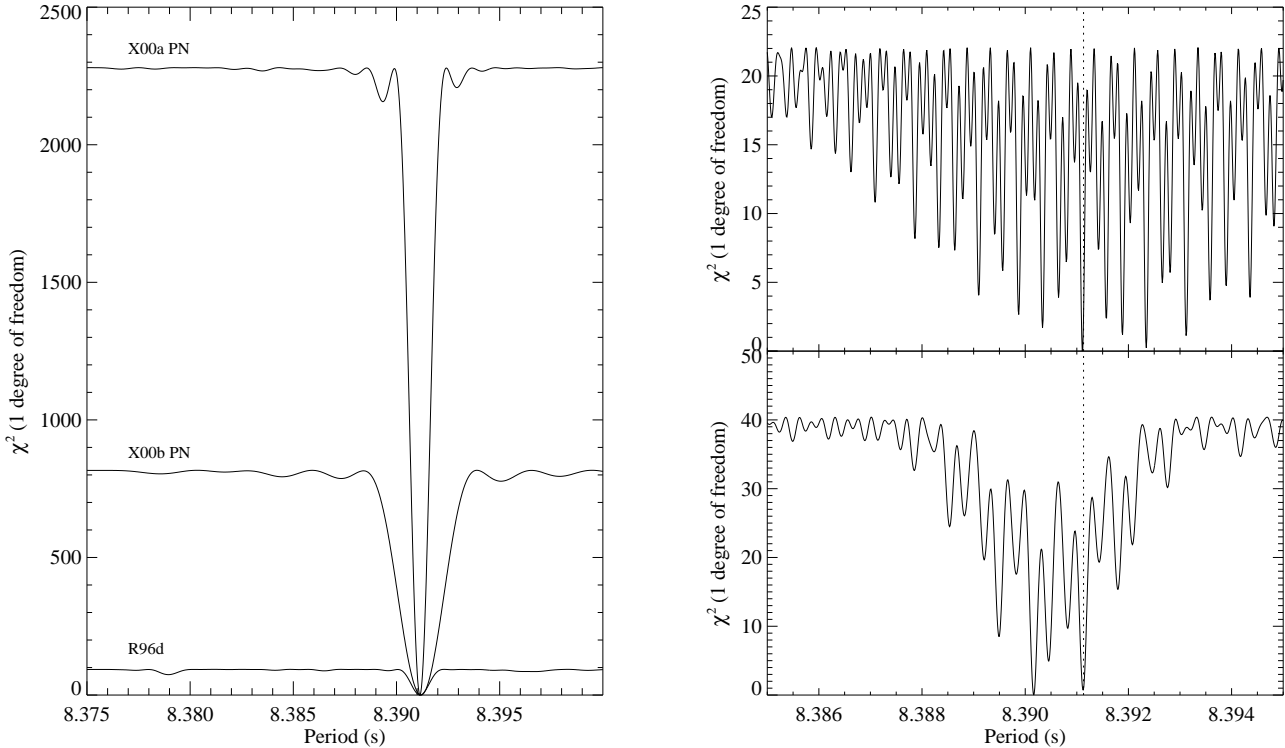


Figure 2. (Left) Maximum likelihood periodogrammes (MLP) for three long datasets, R96d, X00a (PN) and X00b (PN), showing the unambiguous detection of a periodicity at 8.391 s. These constrain the selection of the strongest and second-strongest dips in the MLPs for the R98 and Ch00 datasets respectively (right). The vertical line denotes a period of 8.39113 s. The 68% and 90% confidence levels are at $\chi^2 = 1.0$ and 2.71 for one degree of freedom.

general maximum likelihood technique, which makes no assumptions on the data distribution (Cash 1979, Lampton, Margon & Bowyer 1976). Using this, Cash (1979) defined the C - and ΔC -statistics. The ΔC -statistic (Cash 1979) has the considerable advantage of being distributed as χ^2 , so that the required confidence intervals can be identified directly from the plot.

The maximum likelihood technique depends on a model probability distribution, which must be specified *a priori*. Haberl et al. (1997) and Cropper et al. (2001) find the flux variation of RXJ0720.4-3125 to be almost sinusoidal, so in our particular case we can take a sinusoidal variation superimposed on a mean value as an appropriate model. The single frequency and absence of harmonics in the Rayleigh transform of the X00a PN dataset shown in Figure 1 provides the justification explicitly for this approach. The maximum likelihood is then computed simply as equation (35) of Bai (1992). The normalisation of the model is unimportant, as it results in a constant term in the C -statistic, which then is eliminated in the ΔC -statistic. In our case we have two free parameters: normalised amplitude and phase. In general, when performing maximum likelihood fits, the best fit free parameters have to be determined by whatever method may be most appropriate. However, in the case of sinusoids, as noted by Bai (1992), their orthogonality allows them to be determined directly from the Rayleigh Transform (or Lomb-Scargle periodogramme).

The computation of the ΔC -statistic is therefore only

slightly more complicated than the periodogramme. It starts in the same way, by a scan through period, calculating the Rayleigh Transform to provide the amplitude and phase at each period. Then at each period the maximum likelihood is calculated using equation (35) of Bai (1992). Finally from equations (4) and (7) of Cash (1979), ΔC is simply twice the difference between the maximum likelihood at a particular period, and the maximum value over the whole frequency range. This results in an inverted “periodogramme”, with minimum value of zero. The permitted period range is that between the confidence levels appropriate for χ^2 with the appropriate number of degrees of freedom (1 or 2 depending on whether \dot{P} is included as a parameter – see section 4).

Details of the procedure are given in Appendix A.

With a period of 8.391 s (Haberl et al. 1997), more than 10^7 cycles have elapsed over the time span of our data set. It is therefore essential to incorporate a \dot{P} term in our analysis techniques when combining datasets at different epochs. The search then becomes a (P_0, \dot{P}) search, where P_0 is the period at the start of the first dataset (the 1993 *Rosat* observations), and the instantaneous period $P = P_0 + \dot{P}(t - t_0)$ is computed at each point in the grid. Here t_0 is the time at the start of the R93 run.

As a more general comment, we recommend this maximum likelihood periodogramme (hereafter MLP) for time series analysis. The uncertainty in a period determination is not evident directly from the width of a peak in a power spectrum computed by classical discrete Fourier transform,

Lomb-Scargle periodogramme or Rayleigh transform, as this is set by the window function (*c.f.* Scargle 1982 appendix D). However, it is directly available from the MLP ΔC statistic: the inverted peak from a sinusoidal signal in data with high signal-to-noise ratio will be narrower than the peak from low signal-to-noise data and the χ^2 can be read directly from the vertical axis (see *e.g.* Figure 2). Furthermore, as noted above, the MLP technique requires an appropriate model, which may be unknown *a priori*. In this case the signal can be reconstructed from the harmonic content of the Rayleigh transform or Lomb-Scargle periodogramme, or from the phase folded data, and an appropriate model generated. This model can then be used in the calculation of the MLP, incorporating all of the harmonic information explicitly.

4 MEASURE OF THE SPIN PERIOD

The only measure of P and \dot{P} presented in the literature for RXJ0720.4-3125 was given by Haberl et al. (1997) using *Rosat* data. The period was determined to be 8.39115 ± 0.00002 seconds from the 1996 Nov 3 dataset. Based on a linear fit of the data spanning 3 years, these authors derived a 90 % confidence range of -6.0×10^{-12} to 0.8×10^{-12} for \dot{P} , compatible with no period change.

It is computationally unfeasible to explore this range in the $P_0\dot{P}$ plane in a single analysis of the entire dataset to determine refined values for P_0 and \dot{P} . A reduction in the range is required. This can be accomplished initially by extending the Haberl et al. (1997) analysis to include the *XMM-Newton* data. This is sufficiently accurate to identify the correct peak in the alias patterns in the extended duration R98 and Ch00 data, leading to a further limiting of the permitted range in the $P\dot{P}$ plane. The next stage is a grid search in P and \dot{P} over this restricted range for the 1993 and 1996 combined *Rosat* data only. The final stage is a grid search using all data in the restricted zone for which there are acceptable solutions from this *Rosat* analysis.

4.1 Individual datasets

We begin by performing an MLP assuming $\dot{P} = 0$ on each of the longer pointing (R93, R96d, X00a, X00b) in the period range (8.375-8.400) s, incorporating the value of 8.39115 s found by Haberl et al. (1997). The results are shown in Figure 2 (left). As we can see, there is no ambiguity in the period determinations from the R96d, X00a and X00b datasets; the best fit frequencies and their uncertainties are reported in Table 2. A linear least square fit using the 68% formal errors from the MLP results in a value of $P_0 = 8.39113 \pm 0.00011$ s, $\dot{P} = 0.0 \pm 5.5 \times 10^{-13}$ s/s, where, as throughout, P_0 is referenced to the start of the R93 run.

The proximity in time between the Ch00 and X00a observations, together with the above upper limit in \dot{P} , permits an unambiguous determination of the second highest peak in the Ch00 power spectrum (Figure 2, right). The same is true for the R98 observations, in which the highest peak is selected. Adding these to the linear least squares fit results in a value of $P_0 = 8.39107 \pm 0.00005$ and $\dot{P} = 2.7 \times 10^{-13} \pm 2.5 \times 10^{-13}$. As may be expected, the P_0

Label	JD start (TDB)	Period (s)	68% Uncertainty (s)
R93	2449257.684706	8.391201	0.000450
R96a	2450199.141848	–	
R96b	2450211.010212	–	
R96c	2450354.488187	–	
R96d	2450391.419553	8.391137	0.000063
R98	2450923.523982	8.391109	0.000013
Ch00	2451575.771501	8.391121	0.000020
X00a PN	2451677.604110	8.391133	0.000021
X00a MOS1	2451677.614469	8.391103	0.000043
X00a MOS2	2451677.614474	8.391120	0.000040
X00b PN	2451870.308664	8.391181	0.000050
X00b MOS1	2451870.390808	8.391041	0.000167
X00b MOS2	2451870.390823	8.391032	0.000181

Table 2. Best fit periods to the longer individual datasets, assuming $\dot{P} = 0$.

and \dot{P} are highly correlated. The 68, 90 and 99% confidence intervals are shown in Figure 3.

The duration and high count-rate of the X00a PN run alone provides a strong constraint in the (P_0, \dot{P}) plane. The MLP 68% and 90% confidence intervals are also shown in Figure 3. This indicates that acceptable values for P_0 and \dot{P} lie within the range 8.39106 to 8.39115 s and -1 to $+2 \times 10^{-13}$ s/s, respectively. We checked the effect of a 10^{-7} error in the *XMM-Newton* clock calibration, as reported recently (Kuster, M., 2001, reported at “New Visions of the X-ray Universe in the *XMM-Newton* and *Chandra* Era”). The change in the confidence region is negligible.

4.2 Combined Rosat dataset

The $P_0\dot{P}$ range identified in Figure 3 is sufficiently restricted for an MLP to be performed on the combined 1993 and 1996 *Rosat* datasets. The use of combined datasets requires coherent phasing to be maintained over the whole dataset (coherent phasing was required only *within* each of the individual datasets used until this point). The (P_0, \dot{P}) plane was searched over between $8.39095 \leq P_0 \leq 8.39120$ s, and $-4 \times 10^{-13} \leq \dot{P} \leq 8 \times 10^{-13}$ s/s, exceeding the parameter range for the 90% confidence limits from the linear least squares fit. The resulting 68% and 90% confidence contours break up into small regions (aliases) distributed along lines in the (P_0, \dot{P}) plane. These are also shown in Figure 3

As is evident, there is overlap between the *Rosat* 90% confidence interval contours and the 99% contours of the linear least squares fit to the individual data (but not quite at the 90% level). This overlap region is also consistent with the X00a PN confidence intervals.

4.3 Full dataset

With the further restriction available from the fit to the *Rosat* 1993 and 1996 data subset in Figure 3, a coherent MLP search was made to all of the data (excluding the uncertain R98 run). The search was made for $8.391050 \leq P_0 \leq 8.391150$ s and $-3 \times 10^{-13} \leq \dot{P} \leq 3 \times 10^{-13}$ s/s within the parallel lines $P_0 = a\dot{P} + b$ defined by intercepts

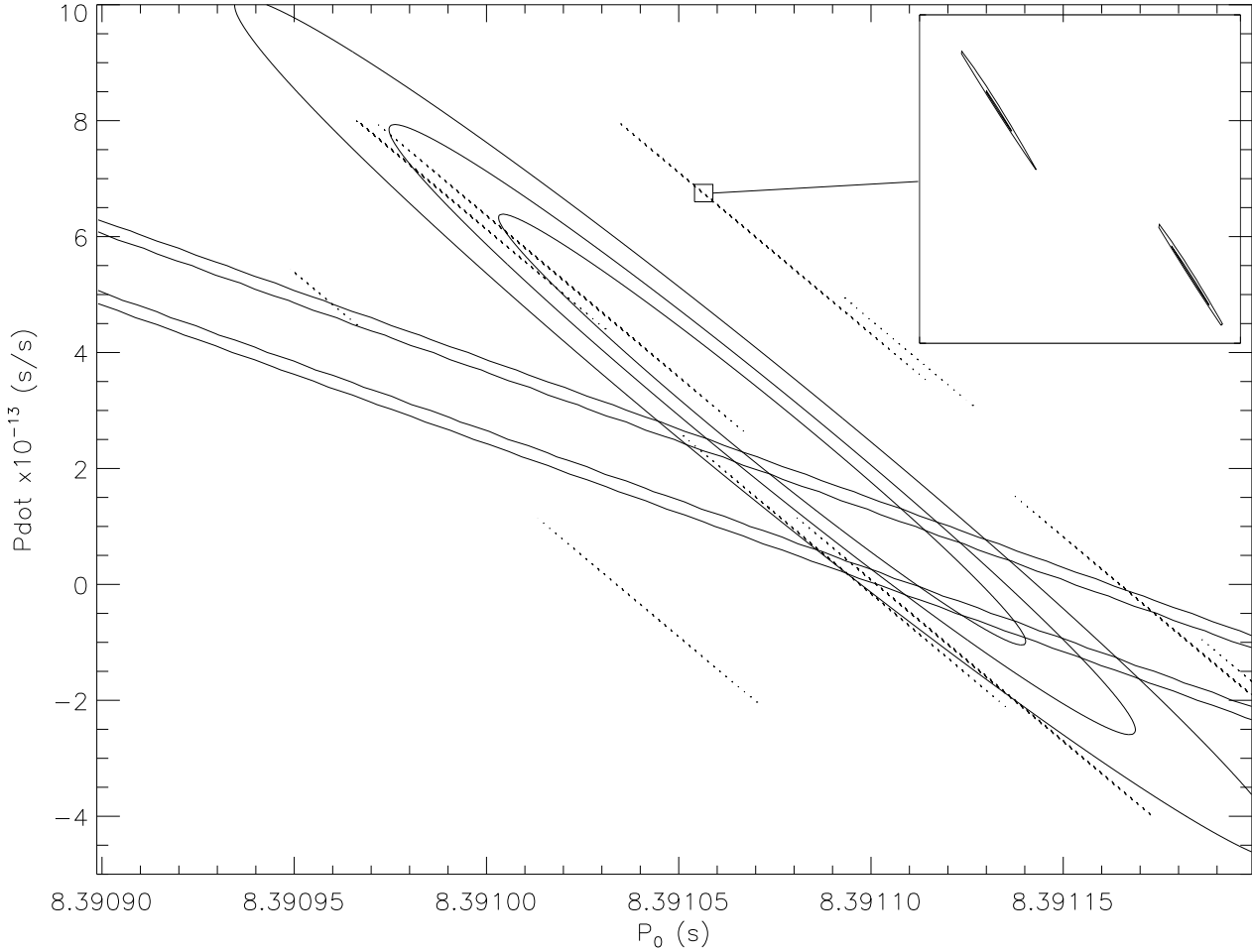


Figure 3. The 68%, 90% and 99% contours for P_0 and \dot{P} linear least squares fit to the individual best fit periods in Table 2 (continuous elliptical regions). Overplotted on the same scale are the 68% and 90% contours from the MLPs to the X00a PN (defined by continuous parallel lines) and the combined 1993 and 1996 *Rosat* datasets. The latter are broken up into tiny elliptical regions corresponding to the 68% and 90% confidence levels for the different aliases: see the enlargement inset in the top right hand part of the figure.

$b = 8.391097$ s and 8.391105 s and slope $a = -1.75 \times 10^8$ s, encompassing the *Rosat* 1993/1996 contours. Care was taken to ensure adequate sampling of the (P_0, \dot{P}) plane. This identified two pairs of values, (P_0, \dot{P}) which cannot be discriminated between on statistical grounds. These are $(P_0, \dot{P}) = 8.39109273$ s, 5.409×10^{-14} s/s and 8.39109148 s, 3.749×10^{-14} s/s (Table 3). All other periods can be excluded at the 95.4% level, but two other possibilities cannot be excluded at the 99% level: these are also given in Table 3 for completeness. The contours for the two best fits are given in Figure 4.

We have folded the data on both $P_0\dot{P}$ solutions (1) and (2) in Table 3 to check that the relative phasing of all individual runs is correct. We show the folded data on these periods in Figure 5. The data from runs R96a and R96b have been combined to increase the signal-to-noise ratio, and we have not shown the data from R98 because of the uncertainty in the time reference for this run (section 2).

Label	P_0 (s)	\dot{P} (s/s)	$\Delta\chi^2$
(1)	8.39109273	5.409×10^{-14}	
(2)	8.39109148	3.749×10^{-14}	1.3
(3)	8.39108624	6.902×10^{-14}	6.2
(4)	8.39108748	8.564×10^{-14}	6.3

Table 3. The four best fit (P_0, \dot{P}) values. Refer to Figure 4 for the confidence interval contours. $\Delta\chi^2$ is the difference between the χ^2 of a given solution, and that of solution (1). Fits (3) and (4) are formally excluded at the 95.4% level.

Now performing the *a posteriori* check with the *BeppoSax* data, we find that these data phase correctly with the main datasets for $P_0\dot{P}$ (1), but not (2). This is shown in the lowest panel of Figure 5 in each case. This allows us to select $P_0\dot{P}$

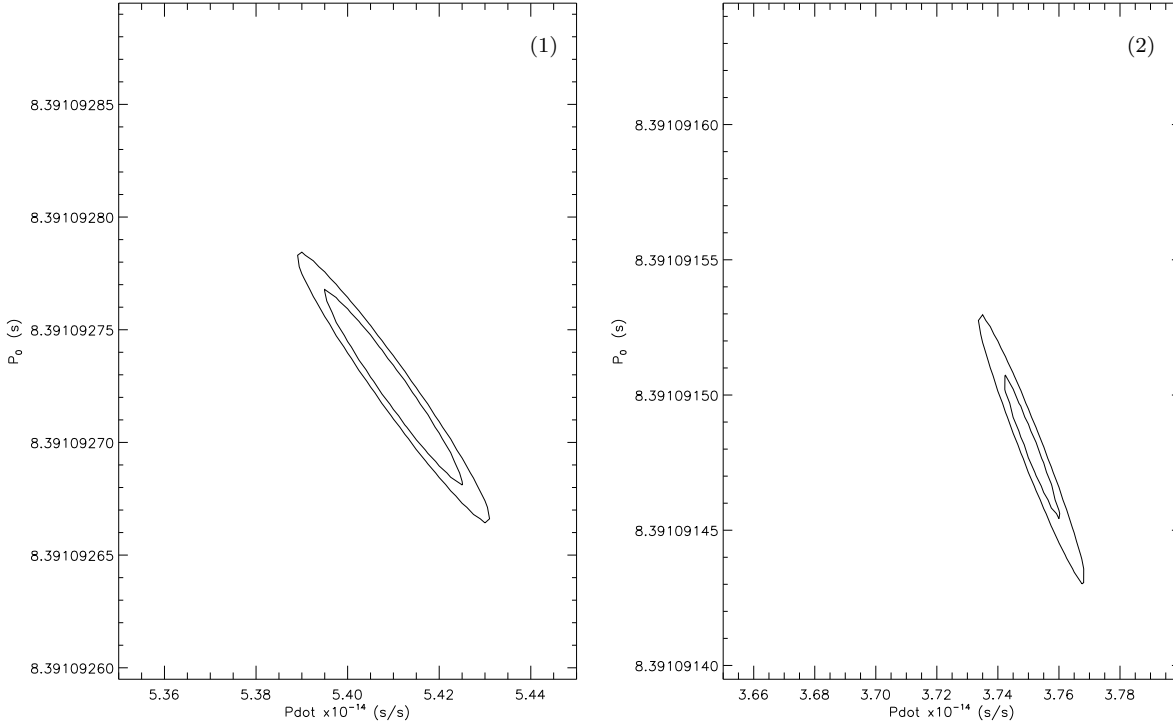


Figure 4. The 68% and 90% MLP contours for P_0 and \dot{P} to the complete dataset except for the R98 data, for the two acceptable (P_0, \dot{P}) values (1) and (2). Note that the contours in (2) are referenced to the best global fit derived for (1).

(1) as the most likely timing parameters for RX J0720.4–3125. In any case, both acceptable fits to the data have $3 \times 10^{-14} < \dot{P} < 6 \times 10^{-14}$. For the purposes of our further discussion, the difference between the \dot{P} in (1) and (2) is not important.

5 DISCUSSION

The refined value of \dot{P} reported in this paper is consistent with, but two orders of magnitude lower than the extrema of the range reported by Haberl et al. (1997). The first implication is that RXJ0720.4-3125 is unlikely to be spinning down under propeller torques. If the propeller is due to the torque exerted by the interstellar medium, it would be (e.g. Colpi et al., 1998)

$$\dot{P}_{prop} \approx 10^{-8} n^{9/13} v_{10}^{-27/13} B_{12}^{8/13} P^{21/13} \frac{\text{s}}{\text{yr}}, \quad (1)$$

where n is the external density in cm^{-3} ($n \sim 1$ for the interstellar medium), $B_{12} = B/(10^{12} \text{ G})$ and v_{10} is the star’s velocity normalized to 10 km/s. By using the values of P and \dot{P} of RXJ0720.4-3125, we obtain $B_{12} \approx 16n^{-9/8} v_{10}^{27/8}$. Propeller spin-down dominates over dipolar losses if $B_{12} < 25\sqrt{n} v_{10}^{-3/2}$ and this, combined with the previous equation, constrains the star’s velocity to extremely small values: $v_{10} \lesssim n^{1/3}$. Moreover, this scenario makes the matching of thermal and dynamical time scales more difficult. On the other hand, the fact that the propeller contribution is negligible supports larger values of the star’s velocity.

In the “unified” model suggested by Alpar (2001), the observed spin-down is associated with propeller effect by a fossil disk. In this case, under the assumption that the X-ray luminosity of the source is supplied by energy dissipation (frictional torque), upper and lower bounds on $\dot{\Omega}$ can be derived by eq.(2) of Alpar (2001). For RXJ0720.4-3125 the observed luminosity is $L \approx 2 \times 10^{31} (d/100 \text{ pc})^2 \text{ erg cm}^{-2} \text{ s}^{-1}$, where $d_{100} = d/100 \text{ pc}$ and d is the distance (Haberl et al. 1997). This gives:

$$2 \times 10^{-12} d_{100}^2 \lesssim \dot{\Omega} \lesssim 2 \times 10^{-10} d_{100}^2 \frac{\text{rad}}{\text{s}^2}, \quad (2)$$

that in turn translates in $\dot{P} = (P^2/2\pi)\dot{\Omega}$

$$2 \times 10^{-11} d_{100}^2 \lesssim \dot{P} \lesssim 2 \times 10^{-9} d_{100}^2 \frac{\text{s}}{\text{s}}. \quad (3)$$

While this scenario is still consistent with the spin-down measured for RBS 1223 (Hambarayan et al., 2002), the value of \dot{P} reported here for RXJ0720.4-3125 is well below this range. Thus, for RXJ0720.4-3125, the associated energy dissipation cannot, alone, account for the source luminosity (unless the source is at $\sim 5 \text{ pc}$, which is unrealistic). That also make less plausible an interpretation of the hardness ratio profile in terms of a spatially variable absorbing matter, co-rotating in the magnetosphere (Cropper et al. 2001). The observed behaviour is more probably explained by the angle-dependent properties of the emitted radiation.

On the other hand, the slow spin-down rate of RXJ0720.4-3125 is still considerable. The other plausible mechanism which may account for such large and stable val-

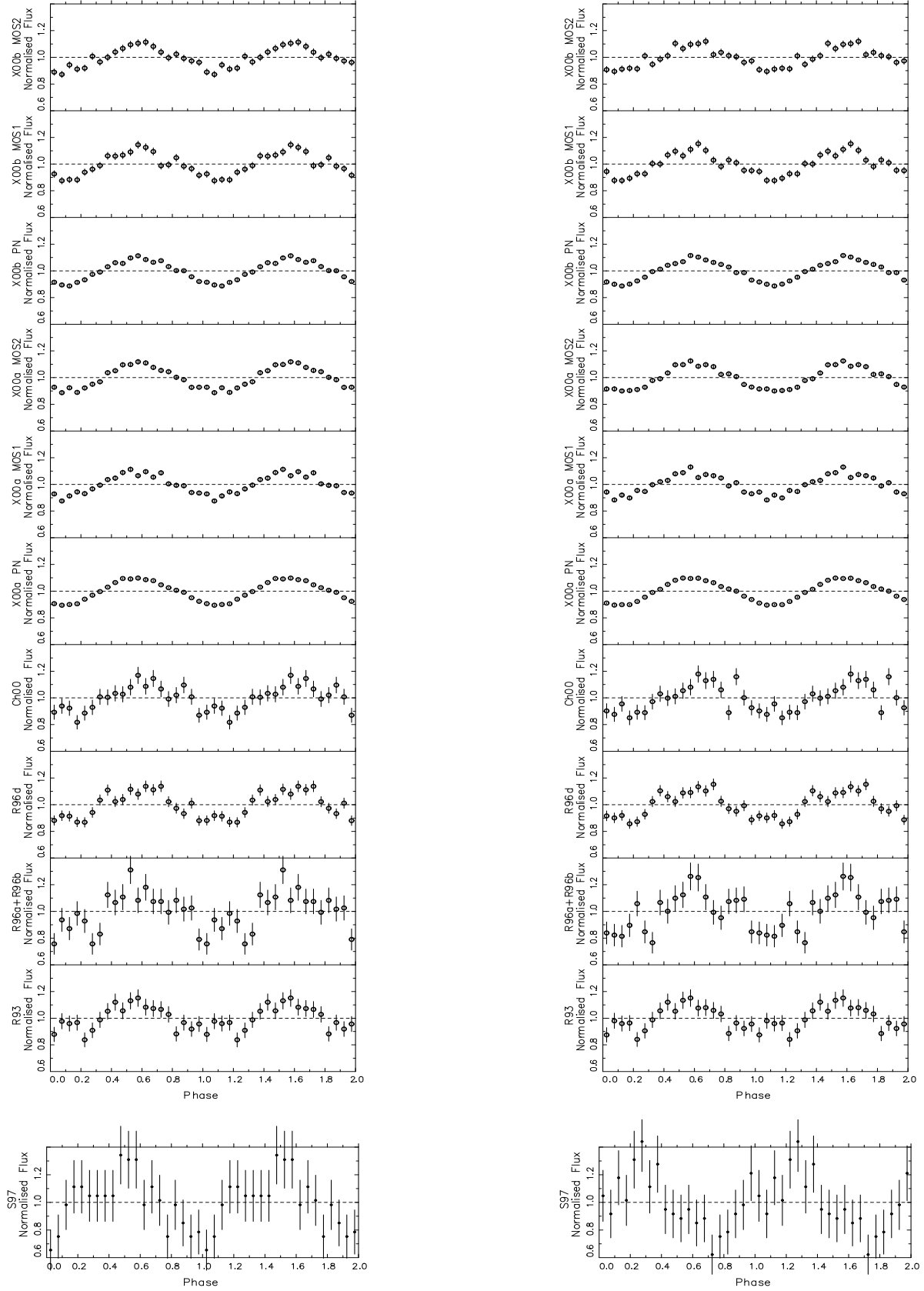


Figure 5. The datasets folded on $P_0\dot{P}$ (1) (left) and (2) (right) in Table 3.

ues of \dot{P} is rotational loss by emission of magnetic radiation. For a dipolar magnetic field,

$$\dot{P} \approx 10^{-15} B_{12}^2 / P \frac{\text{s}}{\text{s}}, \quad (4)$$

which gives a present value of the magnetic field of $B = 2.13 \times 10^{13} \text{ G}^{\dagger\dagger}$. Despite this value being below those typically quoted for magnetars ($B \approx 10^{14} - 10^{15} \text{ G}$), it is still extreme and close to the critical value $B_Q = 4.41 \times 10^{13} \text{ G}$ at which quantizing effects start to be important in shaping the atmospheric emission. Furthermore, a scenario in which this source is powered by accretion from the interstellar medium must be ruled out: for the present values of P and B the corotating magnetosphere will prevent the incoming material to penetrate below the Alfvén radius.

The corresponding spin-down age is

$$t_{sd} = \dot{P} / (2P) \sim 2.48 \times 10^6 \text{ yr}, \quad (5)$$

which, given the numerous uncertainties, is marginally compatible with that inferred by the cooling curves: a few 10^5 yrs for a surface temperature of $\sim 80 \text{ eV}$ (see e.g. Kaminker, Haensel & Yakovlev, 2001, Kaminker, Yakovlev & Gnedin, 2001; Schaab et al. 1997, 1999). The discrepancy is less significant if we notice that: a) the cooling curves are strongly dependent on the neutron star mass (Kaminker, Haensel & Yakovlev, 2001), and b) what we are probably observing in X-rays is a region of limited size which is kept hotter than the average star surface, as inferred by the analysis of the pulse-shape (Cropper et al., 2001).

On the other hand, t_{sd} is representative of the true age of the source only in the case in which the magnetic field remained almost constant during the star evolution. The same condition applies for the validity of the cooling curves mentioned above, which do not include the extra input of energy released in the neutron star in case of field decay. It is therefore of fundamental importance to address the field evolution: the strength of B and its variation during the neutron star history determine, in fact, the actual luminosity, the lifetime and even the nature of the energy loss from the star. A related question is where the field is anchored: in the core, penetrating the whole star or confined in the crust. There are three mechanisms which are typically proposed for inducing field-decay: ambipolar diffusion in the solenoidal or irrotational mode and Hall cascade (Goldreich & Reisenegger 1992, Heyl & Kulkarni 1998, Colpi, Geppert & Page 2000). In reality all the three processes co-exist with different timescales, and each of them may dominate the evolution depending on B , L at any given time. In absence of more detailed computations, Heyl & Kulkarni (1998) and Colpi, Geppert & Page (2000) tentatively isolated the three processes and proposed some simple, phenomenological rules to mimic the evolution in the three regimes. We stress that these descriptions are far from being comprehensive of all the effects that can modify substantially the results: they are used in a first approximation and have the main advantage

[†] Note that a twisted magnetosphere may lead to a reduction up to an order of magnitude in the inferred polar value of the magnetic field. The considerations about the age, however, remain unchanged (Thompson, Lyutikov & Kulkarni, 2001).

^{††} Here and in the following we specify the discussion to solution (1) of Table 3

B-Decay Mechanism	B_0 10^{13} G	age (years)
Hall Cascade	119.2	4.5×10^4
Ambipolar diffusion, irrotational mode	1.9	3.3×10^6
Ambipolar diffusion, solenoidal mode	4.1	1.6×10^6

Table 4. Predicted source age and primordial field for three different mechanisms of decay, simulated as in Colpi et al. (2000). The present values of P and \dot{P} are those of solution (1) in table 3. In all cases, the source is assumed to be born with $P = 1 \text{ ms}$.

of having a simple analytical form. By using the expressions of Colpi et al. (2000), we have estimated the source age and the value of the magnetic field at the birth of the neutron star, B_0 . Results are shown in Table 4. In all cases the star is assumed to be born with a period of 1 ms: results are not strongly dependent on this exact value, provided it is far less than the present period.

As we can see, allowing for a mechanism involving very fast decay, such as the Hall cascade, we find that the source is now $\sim 4 \times 10^4$ yr old, and is born with a superstrong field $B_0 \sim 10^{15} \text{ G}$. Such a young age is only marginally compatible with the absence of a remnant and, more important, is not compatible with the low observed X-ray luminosity (as we compared using not only the standard cooling curves mentioned above, but also some cooling curves kindly provided by Geppert & Colpi, private communication; these latter are computed allowing for the extra-heating due to B -decay from Hall cascade and predict larger luminosities than the former, making the discrepancy even higher). Underluminous models have been recently presented by Kaminker, Haensel & Yakovlev (2001), who accounted for the enhanced neutrino cooling in presence of strong neutron superfluidity. These solutions may match an age of $\sim 10^4$ yrs for RXJ0720.4-3125, but, as discussed by the same authors, they must probably be rejected since they fail in the comparison with observational data of a sample of other neutron stars.

On the other hand, both mechanisms involving ambipolar diffusion predict a magnetic field quite stable over the source lifetime and close to the actual value. Accordingly, the predicted age is $\sim 10^6$ years in all cases, close to t_{sd} . Below $\sim 10^{14} \text{ G}$ the cooling curves are not significantly influenced by decay through ambipolar diffusion (Heil & Kulkarni, 1998), thus, as in the case of constant B discussed above, the scenario is compatible with the observed luminosity. The larger age is also compatible with the absence of a remnant.

If our conclusions are valid, the connection between dim INS and AXPs is not so obvious. RXJ0720.4-3125 has a strong, but not superstrong, field which is compatible with those of the canonical radio-pulsars which have passed the death line. On the other hand, having excluded accretion, what mechanism causes an X-ray emission concentrated in a fraction of $\sim 60\%$ of the star surface remains a mystery, as well as the related question about the validity of using the observed blackbody temperature to locate the source in the cooling diagram. The variation of the surface cooling temperature with the latitude predicted so far for strong fields is not large enough and more complicated explanations are required.

6 ACKNOWLEDGEMENTS

We are grateful to Mat Page for his advice on the maximum likelihood methods, and to Darragh O'Donoghue for pointing us to the Raleigh transform, and for the use of his Eagle Fourier transform code used in the preliminary stages of this work. We are grateful to Monica Colpi for lots of useful discussion, to Ulrich Geppert for providing the cooling curves and to Sandro Mereghetti for reading the manuscript.

REFERENCES

- Alpar, M. A. 1999, astro-ph/9912228
 Alpar, M. A. 2000, astro-ph/0005211
 Alpar, M. A. 2001, ApJ, 554, 1245
 Alpar, M. A., Anay, A. & Yazgan, E. 2001, ApJ, 557, L61
 Bai, T., 1992, ApJ, 397, 584
 Cash, W., 1979, ApJ, 228, 939
 Colpi, M., Turolla, R., Zane, S., & Treves, A., 1998, ApJ, 501, 252
 Colpi, M., Geppert, U. & Page, D., 2000, ApJ, 529, L29
 Cropper, M., Zane, S., Ramsay, G., Haberl, F. & Motch, C., 2001, A&A, 365, L302
 Deeming, T. J., 1975, it Astrophys. Space Sci., 36, 137
 de Jager, O. C., 1991, ApJ, 378, 286
 Greenstein, G. & Hartke, G.J., 1983, ApJ, 271, 283
 Goldreich, P. & Reisenegger, A., 1992, ApJ, 395, 250
 Haberl, F., Motch, C., Buckley, D. A. H., Zickgraf, F.-J., Pietsch, W., 1997, A&A, 326, 662
 Hambaryan, V., Hasinger, G., Schwobe, A.D. & Schulz, N.S., 2002, A&A, 381, 98
 Heyl, J.S. & Kulkarni, S.R., 1998, ApJ, 506, L61
 Heyl, J.S. & Hernquist, L., 1998, MNRAS, 297, L69
 Kulkarni, S.R., & van Kerkwijk, M.H. 1998, ApJL, 507, L49
 Kaminker, A.D., Haensel, P. & Yakovlev, D.G., 2001, A&A, 373, L17
 Kaminker, A.D., Yakovlev, D.G. & Gnedin, O.Y., 2001, A&A submitted (astro-ph/0111429)
 Kouveliotou, C. et al. 1998, Nature, 393, 235
 Kouveliotou, C. et al. 1999, ApJL, 510, L115
 Kurtz, D. W., 1985, MNRAS, 213, 773
 Lampton, M., Margon, B., Bowyer, S., 1976, ApJ, 208, 177
 Mardia, K. V., 1972, Statistics of Directional Data (London:Academic)
 Mereghetti, S., in The Neutron Star-Black Hole Connection, eds. V. Connaughton, C. Kouvelioyu, J. Van Paradijs & J. Ventura (NATO-ASI), p.351
 Motch, C. 2001, in "X-ray astronomy: Stellar Endpoints, AGN, and the Diffuse X-ray Background", AIP Conference Proceedings Vol. 599, p244, Eds. N.E. White, G. Malaguti, G.G.C. Palumbo.
 Motch, C., & Haberl, F. 1998, A&A, 333, L59
 Paerels, F., Mori, K., Motch, C., Haberl, F., Zavlin, V.E., Zane, S., Ramsay, G., Cropper, M., 2001, A&A, 365, 302
 Page, D., 1995, ApJ, 442, 273
 Pavlov, G.G., Zavlin, V.E., Trümper, J. & Neuhäuser, R., 1996, ApJ, 472, L33
 Perna, R., Heyl, J.S., Hernquist, L.E., Juett, A.M., Chakrabarty, D., 2001, ApJ, 557, 18
 Schaab, C., Voskresensky, D., Sedrakian, A. D., Weber, F. & Weigel, M. K., 1997, A&A, 321, 591
 Schaab, C., Sedrakian, A., Weber, F. & Weigel, M. K., 1999, A&A, 346, 465
 Scargle, J. D., 1982, ApJ, 263, 835
 Schwarzenberg-Czerny, A., 1998, MNRAS, 301, 831
 Thompson, C., Lyutikov, M. & Kulkarni, S.R., 2001, ApJ submitted (astro-ph/0110677)

- Treves, A., Turolla, R., Zane, S., Colpi, M., 2000, PASP, 112, 297
 Zane, S., Turolla, R., Stella, L. & Treves, A., 2001, ApJ, 560, 384

APPENDIX A: DETAILS OF THE MAXIMUM LIKELIHOOD PERIODOGRAMME

The C -statistic is derived from the maximum likelihood ratio and is

$$C = 2(E - \sum_{i=1}^N n_i \ln I_i) \quad (\text{A1})$$

(Cash 1979), where E is the sum of the expected number of counts according to the model distribution, n_i is the observed number of counts in an interval and I_i is the expected number of counts at the time of event t_i according to the model distribution. N is the total number of counts. For event list data, the sampling duration tends to zero and $n_i = 1$. The ΔC -statistic is

$$\Delta C = (C_{min})_{p-q}^T - (C_{min})_p \quad (\text{A2})$$

where p is the total number of parameters, and q is the number of free parameters. This is distributed as χ^2 with q degrees of freedom (Cash 1979). $(C_{min})_p$ is the minimum C -statistic when all parameters are varied – the minimum over all points in the search grid in the free parameter space. $(C_{min})_{p-q}^T$ is the minimum C -statistic at any particular point in the search grid. Substituting,

$$\Delta C = 2 \left[\left(\sum_{i=1}^N n_i \ln I_i \right)_{best} - \left(\sum_{i=1}^N n_i \ln I_i \right)_{particular} \right] \quad (\text{A3})$$

The expected number of counts I_i in equation (A1) is calculated from the model distribution. In our case of a pure sinusoidal variation, because the expected arrival of an event is directly proportional to the model prediction for time t_i , we have

$$I_i = a_0(1 + A \cos(2\pi t_i/P + \theta_0)) \quad (\text{A4})$$

where A is the normalised amplitude, P is the period and θ_0 is the phase. The scaling of this model a_0 is unimportant, as constant factors are eliminated when substituting in equation (A3). This model has parameters (A, P, θ_0) so $p = 3$. The periodogramme will scan in P , with best fit values for A and θ_0 , so $q = 1$. In the case where we allow a period change,

$$P = P_0 + \dot{P}t_i \quad (\text{A5})$$

where P_0 is the period at $t_i = 0$ and \dot{P} is the period change, the periodogramme will consist of a scan in P_0 and \dot{P} . In this case $p = 4$ and $q = 2$.

In the general case of a maximum likelihood statistic, an optimisation search is required to obtain the best fit for the $p - q$ fitted parameters. Here, in the case of a sinusoid, these can be derived directly from the Rayleigh transform, as pointed out by Bai (1992),

$$z = \frac{1}{N} \left[\left(\sum_{i=1}^N n_i \cos 2\pi t_i/P \right)^2 + \left(\sum_{i=1}^N n_i \sin 2\pi t_i/P \right)^2 \right] \quad (\text{A6})$$

where z is the Rayleigh power, and again, $n_i = 1$ for event list data. The amplitude is then

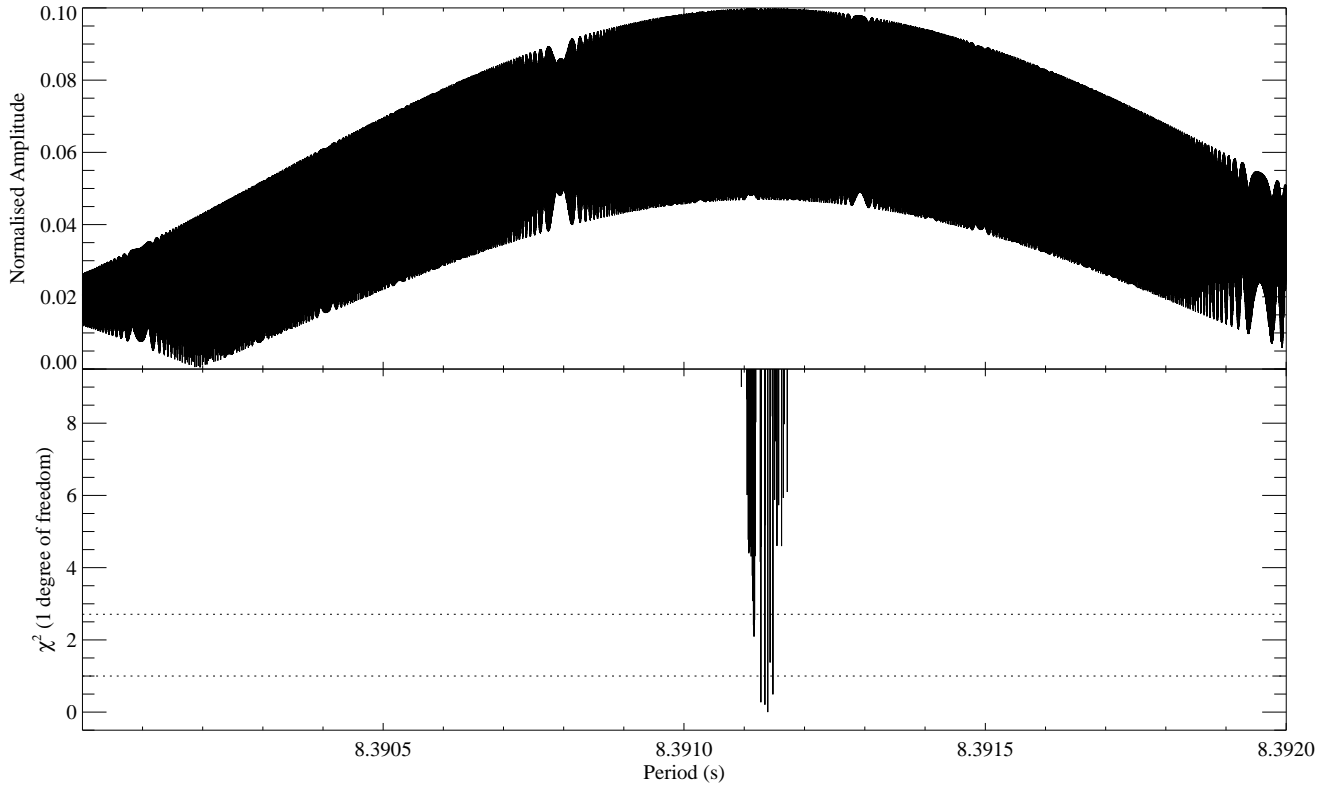


Figure 6. The discrete Fourier transform (top) and maximum likelihood periodogram (bottom) for the X00a PN and X00b PN data over a restricted period range around the 8.391 s period in RXJ0720.4-3125. The 68% and 90% confidence levels are indicated at $\chi^2 = 1.0$ and 2.71 for one degree of freedom.

$$A = 2\sqrt{z/N} \quad (\text{A7})$$

and the phase is

$$\theta_0 = \arctan \left[\left(-\sum_{i=1}^N n_i \sin 2\pi t_i / P \right) / \left(\sum_{i=1}^N n_i \cos 2\pi t_i / P \right) \right]. \quad (\text{A8})$$

This is equivalent numerically to the discrete Fourier transform (DFT) (Deeming (1975), as can be ascertained by reference to Kurtz (1985), equation (A2).

The procedure is then for each P (which may be calculated from equation (A5) in a P_0, \dot{P} search) to calculate the amplitude and phase through equations (A7) and (A8) (which amounts to calculating the Rayleigh or discrete Fourier transform), then calculate ΔC through equations (A4) and (A3). As the P grid is searched, the maximum $\sum n_i \ln I_i$ is stored: ΔC is then simply twice the difference between the calculated value at each period, and this recorded maximum. This difference is distributed as χ^2 for one or two degrees of freedom, depending on whether P is used directly, or calculated in a (P_0, \dot{P}) search through equation (A5).

An illustration of the power of the MLP is given in Figure 6. Here we have taken the X00a PN and X00b PN data, and computed a discrete Fourier transform in the narrow period range 8.390 to 8.392 s (a much expanded scale by comparison with Figure 2), assuming no \dot{P} . This (upper plot) shows a multiplicity of aliases created by the long gap in the data, superimposed on the broad peak corresponding to the duration of the longest observation (X00a). These are

barely resolved in the plot. The lower plot is the MLP with the 68% and 90% confidence levels indicated. This eliminates most of the aliases, as the narrowness of the distribution is related to the precision with which the best fit period can be identified within the broad peak in the upper plot. In the case of the high signal-to-noise ratio X00a and X00b data, this is significantly narrower than the width of the peak, which is set by the window function (Scargle 1982).